AGU PUBLICATIONS

Global Biogeochemical Cycles

RESEARCH ARTICLE
10.1002/2013GB004668

Key Points:
- Description of phytoplankton growth colimitation by nutrients and light
- Prediction of phytoplankton cellular quotas of N, P, and Chl

Correspondence to:
L. Arteaga,
larteaga@geomar.de

Citation:
Arteaga, L., M. Pahlow, and A. Oschlies (2014), Global patterns of phytoplankton nutrient and light colimitation inferred from an optimality-based model, *Global Biogeochem. Cycles*, *28*, doi:10.1002/2013GB004668.

Received 5 JUN 2013
Accepted 11 JUN 2014
Accepted article online 13 JUN 2014

Global patterns of phytoplankton nutrient and light colimitation inferred from an optimality-based model

Lionel Arteaga[1], Markus Pahlow[1], and Andreas Oschlies[1]

[1]GEOMAR Helmholtz Centre for Ocean Research Kiel, Kiel, Germany

Abstract The widely used concept of constant "Redfield" phytoplankton stoichiometry is often applied for estimating which nutrient limits phytoplankton growth in the surface ocean. Culture experiments, in contrast, show strong relations between growth conditions and cellular stoichiometry with often substantial deviations from Redfield stoichiometry. Here we investigate to what extent both views agree by analyzing remote sensing and in situ data with an optimality-based model of nondiazotrophic phytoplankton growth in order to infer seasonally varying patterns of colimitation by light, nitrogen (N), and phosphorus (P) in the global ocean. Our combined model-data analysis suggests strong N and N-P colimitation in the tropical ocean, seasonal light, and N-P colimitation in the Northern Hemisphere, and strong light limitation only during winter in the Southern Ocean. The eastern equatorial Pacific appears as the only ocean area that is essentially not limited by N, P, or light. Even though our optimality-based approach specifically accounts for flexible stoichiometry, inferred patterns of N and P limitation are to some extent consistent with those obtained from an analysis of surface inorganic nutrients with respect to the Redfield N:P ratio. Iron is not part of our analysis, implying that we cannot accurately predict N cell quotas in high-nutrient, low-chlorophyll regions. Elsewhere, we do not expect a major effect of iron on the relative distribution of N, P, and light colimitation areas. The relative importance of N, P, and light in limiting phytoplankton growth diagnosed here by combining observations and an optimal growth model provides a useful constraint for models used to predict future marine biological production under changing environmental conditions.

1. Introduction

Attempts to construct a synthesis of global marine production and its impacts on global biogeochemical cycles often rely on the assumption of constant elemental stoichiometry of phytoplankton (Redfield stoichiometry, [*Redfield*, 1934]). While convenient and roughly consistent with globally averaged relations inferred from biogeochemical tracer distributions [*Fanning*, 1992], the assumption of constant elemental stoichiometry is at odds with observed temporal and regional variations of elemental composition of phytoplankton and associated biogeochemical fluxes [*Geider and LaRoche*, 2002; *Körtzinger et al.*, 2001]. Carbon:nitrogen:phosphorus (C:N:P) ratios are observed to vary widely among different groups of phytoplankton [*Quigg et al.*, 2003; *Klausmeier et al.*, 2004] and in response to nutrient and light limitation [*Flynn*, 2010; *Healey*, 1985; *Laws and Bannister*, 1980].

There is no clear physiological reason why C:N:P ratios of phytoplankton should strictly adhere to any particular stoichiometry (e.g., Redfield stoichiometry, [*Geider and LaRoche*, 2002]). Although the molar Redfield N:P ratio of 16 is commonly used as a threshold indicating either N or P limitation [*Fanning*, 1992; *Goldman et al.*, 1979], we are not aware of any direct evidence that a N:P ratio of 16 separates N and P limitation of phytoplankton growth. On the contrary, chemostat experiments suggest that the transition from N to P limitation occurs at N:P supply ratios of about 30 [*Rhee*, 1978]. This leads to the conclusion that previous methods for inferring N or P limitation in the surface ocean may need to be revised.

The ratio of dissolved inorganic N:P (DIN:DIP) in the ocean (mainly NO_3^-, NH_4^+, and PO_4^{3-}) results from the balance of nutrient supply from below and differential utilization by phytoplankton and bacteria within the euphotic zone. Shifts in phytoplankton optimal N:P will likely induce alterations in the DIN:DIP ratio [*Weber and Deutsch*, 2012]. Empirical cell quota models [*Droop*, 1983] are capable of decoupling C, N, and P, while optimality-based models of phytoplankton growth offer the potential to help understand the interrelations between phytoplankton stoichiometry and primary production in the ocean [*Smith et al.*, 2011]. Recently,

Table 1. Model Parameters Values and Settings for the Sensitivity Experiments

Symbol	Default	Case I	Case II	Description
A_0	0.7	1	0.06	Potential nutrient affinity (m^3 mmol C^{-1} d^{-1})
α	0.7	0.5	3.7	Chl-specific light absorption coefficient (m^2 mol C E^{-1} g Chl $^{-1}$)
Q_0^N	0.046	0.1	0.026	Subsistence N:C (mol N mol C $^{-1}$)
Q_0^P	0.0016	0.0008	0.0027	Subsistence P:C (mol P mol C $^{-1}$)
R_M^{Chl}	0.1	0.1	0.1	Cost of Chl maintenance (d^{-1})
ζ^{Chl}	0.4	0.3	0.6	Cost of photosynthesis coefficient (mol C g Chl^{-1})
ζ^N	0.6	1	0.7	Cost of DIN uptake (mol C mol N^{-1})
V_0^C, V_0^N, V_0^P				Potential C, N, and P acquisition rates dependent on temperature: 1.4×1.066^{TEMP} (mol C, N, P mol C^{-1})

the behavior of Droop's cell quota model [*Droop*, 1983] could be related to that of optimality-based models [*Pahlow and Oschlies*, 2013].

Here we use an optimality-based model of phytoplankton growth [*Pahlow et al.*, 2013] as a mechanistic foundation for the physiological regulation of nutrient acquisition and light harvesting to diagnose N, P, and light limitation, based on field and satellite data of nutrients, light, and temperature in the surface ocean. One aim of this study is to investigate to what extent the results of this combined model-data analysis are consistent with earlier more pragmatic attempts [*Fanning*, 1992] that infer limiting factors from an analysis of surface DIN:DIP with respect to the Redfield ratio.

2. Methods

In order to estimate N, P, and light colimitation in the global ocean, we calculated the light-limited steady state solution of the optimality-based chain model of *Pahlow et al.* [2013], modified to allow for temperature dependence (see Appendix A). The model was forced with nutrient, light, and temperature data of the surface mixed layer derived from the World Ocean Atlas 2009 (WOA09) database (http://www.nodc.noaa.gov/OC5/WOA09/pr_woa09.html) and satellite observations from the Moderate Resolution Imaging Spectroradiometer (MODIS) (at http://oceancolor.gsfc.nasa.gov/), using the Default parameters in Table 1. Temperature, surface nitrate, and phosphate concentrations were obtained as monthly means from WOA09 on a 1° resolution spatial grid. While there are other sources of bioavailable N and P, nitrate and phosphate are the dominant forms and we believe they can serve to describe the general picture of nondiazotrophic phytoplankton growth (co)limitation by N and P in the global ocean. Mixed layer depth (MLD) was defined as the depth at which density exceeds surface density by 0.125 kg m^{-3} [*Levitus*, 1982]. Density was calculated from global gridded (1°) monthly temperature and salinity data from WOA09.

Light was estimated as "median mixed layer light level" (I_g) [*Behrenfeld et al.*, 2005],

$$I_g = \frac{1}{D} \cdot \mathrm{PAR} \cdot e^{-K490 \cdot \frac{\mathrm{MLD}}{2}} \tag{1}$$

I_g depends on the day-length-fraction (D, given by the time of the year), surface photosynthetically active radiation (PAR)(E m^{-2} d^{-1}), the diffusive light attenuation coefficient estimated at 490 nm (K490) (m^{-1}) and MLD (m) [*Behrenfeld et al.*, 2005]. Surface PAR and K490 were obtained from MODIS and regridded to a 1° resolution spatial grid. Owing to the saturation of photosynthesis at relatively low light intensities compared to surface PAR, I_g yields a better representation of light limitation of photosynthesis (see S_i below) than the mean mixed layer light level, which strongly overestimates average mixed layer photosynthesis. The WOA09 compilation represents monthly mean values of data collected over many years, whereas satellite data were obtained as monthly means specifically for the period between January 2005 and December 2010 and averaged into a monthly "climatology" in order to match the temporal resolution of the WOA09 data set.

2.1. Optimality-Based Chain Model

The chain model of *Pahlow et al.* [2013] is a phytoplankton cell quota growth model. The model defines the physiological roles of N and P based on their association with specific functional cellular compartments [*Sterner and Elser*, 2002], whereby net C fixation (phytoplankton growth) is directly limited by cellular N. N is associated with enzyme activity, thus controlling major cellular metabolic processes and limiting growth

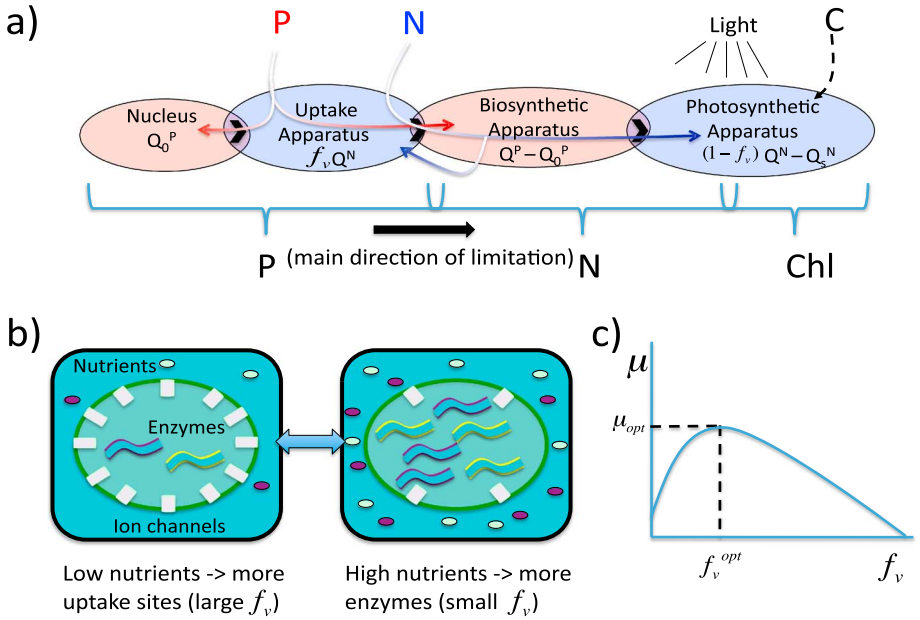

Figure 1. (a) Chain model compartments and associated partial nutrient quotas for N and P: P is associated with the nucleus (Q_0^P) and the biosynthetic apparatus ($Q^P - Q_0^P$). N is associated with the nutrient uptake apparatus ($f_V\, Q^N$) and the photosynthetic apparatus ($(1 - f_V)(Q^N - Q_s^N)$). In the model dynamics P limits N acquisition, while N limits Chl synthesis and C fixation. (b) Optimal allocation of N maximizes nutrient (N and P) assimilation: A greater N quota fraction (f_V) is allocated for nutrient acquisition under low extracellular nutrient concentration. Under high-nutrient conditions a greater N fraction is preferentially allocated for carbon fixation. (c) Net cell growth (μ) is maximized via optimization of f_V (see Appendix A for details).

rate via C fixation and light harvesting. In the case of nitrate and nitrite, inorganic N first has to be reduced to ammonium before it is assimilated into protein. N assimilation occurs in the biosynthetic apparatus (ribosomes) and is constrained by P, which is a major component of ribosomes. In this way P limits N acquisition and N limits C fixation [*Ågren*, 2004]. The model optimizes the allocation of cellular N and energy among requirements for nutrient acquisition and light harvesting to maximize growth rate for the given inorganic nutrient concentrations and light availability (Figure 1) (see Appendix A for details). The present analysis aims to describe N, P, and light (co)limitation of a nondiazotrophic phytoplankton.

2.2. Cell Quota, Nutrient and Light Limitation Estimates

Limitation is here defined as the effect of light and nutrients on phytoplankton growth rate. Nutrient limitation is estimated from phytoplankton cell quotas of N (Q_N = N:C) and P (Q_P = P:C) in the surface mixed layer as diagnosed from the model and the relative difference with respect to the N and P subsistence quotas Q_0^N and Q_0^P (i.e., the lowest N:C and P:C ratios that the cells can assume in the model (Table 1)). N:C molar ratios can vary from about 0.04 (C:N = 25 mol mol^{-1}) in low nutrient conditions to over 0.2 (C:N = 5 mol mol^{-1}) in nutrient replete conditions [*Geider and LaRoche*, 2002], while P:C can vary between roughly 0.002 and 0.01 (C:P = 500 and 10 mol mol^{-1}) [*Terry et al.*, 1985; *Healey*, 1985].

Photosynthetically active radiation is represented here by the median mixed layer light level (I_g, equation (1)). In the model I_g is used as the light intensity reaching the photosynthetic apparatus in the chloroplast. The effect of light limitation is then quantified by the degree of light saturation of the cellular light-harvesting apparatus [S_I, *Pahlow*, 2005],

$$S_I = 1 - e^{-\frac{\alpha I_g \hat{\theta}^C}{V_0^C}} \tag{2}$$

where α is the light absorption coefficient, V_0^C is the potential C fixation rate, and $\hat{\theta}^C$ is the chlorophyll to carbon ratio of the chloroplast.

In order to obtain a quantitative assessment of nutrient (N and P) and light colimitation, we define limitation indices based on nutrient cell quotas and light saturation. The nutrient limitation index (L_{nutrient})

is defined by the relative difference between actual cell quota Q^{nutrient} and subsistence cell quota Q_0^{nutrient} via

$$L_{\text{nutrient}} = 1 - \frac{Q^{\text{nutrient}} - Q_0^{\text{nutrient}}}{Q^{\text{nutrient}}} = \frac{Q_0^{\text{nutrient}}}{Q^{\text{nutrient}}} \tag{3}$$

with $L_{\text{nutrient}} = 1$ for $Q^{\text{nutrient}} = Q_0^{\text{nutrient}}$ indicating strong limitation and zero growth, and L_{nutrient} declines for large cell quotas under nutrient replete conditions. The light limitation index (L_{I}) is defined in an analogous manner as one minus the degree of light saturation of the cellular light-harvesting apparatus, i.e.,

$$L_{\text{I}} = 1 - S_{\text{I}} \tag{4}$$

and serves as an indicator of light limitation experienced by the cells in the mixed layer.

2.3. Estimation of the Chlorophyll to Carbon Ratio

The chlorophyll to carbon (Chl:C) ratio combines the effects of nutrient and light limitation driven by the growth requirements of the cell [*Cullen and Lewis*, 1988]. The Chl:C ratio is regulated to maximize the energy available for N assimilation [*Pahlow et al.*, 2013]. First, the Chl:C ratio of the chloroplast ($\hat{\theta}^{\text{C}}$) is obtained via

$$\hat{\theta}^{\text{C}} = \frac{1}{\zeta^{\text{Chl}}} + \frac{V_0^{\text{C}}}{\alpha I_g}\left\{1 - \text{W}_0\left[\left(1 + \frac{R_{\text{m}}^{\text{Chl}}}{DV_0^{\text{C}}}\right)\text{e}^{\frac{\alpha I_g}{V_0^{\text{C}}\zeta^{\text{Chl}}}+1}\right]\right\} \quad \text{if} \quad I_g > I_{g_0} \tag{5}$$

$$\hat{\theta}^{\text{C}} = 0 \quad \text{if} \quad I_g \le I_{g_0}$$

where ζ^{Chl} is the cost of photosynthesis, $R_{\text{m}}^{\text{Chl}}$ is the cost of Chl maintenance, and W_0 is the 0 branch of the Lambert W function, and

$$I_{g_0} = \frac{\zeta^{\text{Chl}} R_{\text{m}}^{\text{Chl}}}{D\alpha} \tag{6}$$

is the threshold irradiance for chlorophyll synthesis.

The Chl:C ratio of the entire cell is then obtained as a direct result of N and light limitation, represented by Q^{N} and $\hat{\theta}^{\text{C}}$, respectively,

$$\text{Chl:C} = \hat{\theta}^{\text{C}}\left(1 - \frac{Q_s^{\text{N}}}{Q^{\text{N}}} - f_{\text{v}}\right) \tag{7}$$

where Q_s^{N} is the partial N quota bound in structural protein, and f_{v} is the fraction of Q^{N} allocated for nutrient acquisition [*Pahlow et al.*, 2013].

3. Results and Discussion

3.1. Nitrogen and Phosphorus Cell Quota

To be consistent with the literature on biogeochemical fluxes, we report our global model-based results as C:N and C:P ratios. The phytoplankton C:N ratio inferred from our seasonally resolved data model analysis (Figures 2a–2d) shows permanently relatively high values of about 20 mol mol^{-1} in the subtropical ocean between 40°N and 40°S. The eastern equatorial Pacific, however, shows lower C:N ratios throughout all seasons, of about 10 mol mol^{-1}. High Northern Hemisphere latitudes display stronger seasonal variability, with relatively low C:N (~5 mol mol^{-1}) between January and March. C:N ratios increase in April–June and are highest in July–September approaching values close to 10 mol mol^{-1} (Figures 2a–2d). In autumn, nitrate concentrations increase and light declines, and phytoplankton C:N ratios at high northern latitudes decrease again during October–December. The Southern Ocean shows much less clear seasonality, with permanently low C:N ratios of around 5 mol mol^{-1}. Overall, there is a clear latitudinal gradient of low to high C:N ratios from high to low latitudes, which is consistent with recent observations [*Martiny et al.*, 2013a].

Patterns of diagnosed phytoplankton C:P ratios also show a clear latitudinal trend with low C:P ratios at high latitudes and high C:P in low latitudes (Figures 2e–2h). Nonetheless, our predicted C:P ratios display also stronger longitudinal variability, with high values in the western North Pacific and particularly the North Atlantic, where the highest C:P is around 450 mol mol^{-1} during July–September (Figure 2g), reflecting essentially depleted phosphate concentrations in this area [*Wu et al.*, 2000]. The remaining tropical

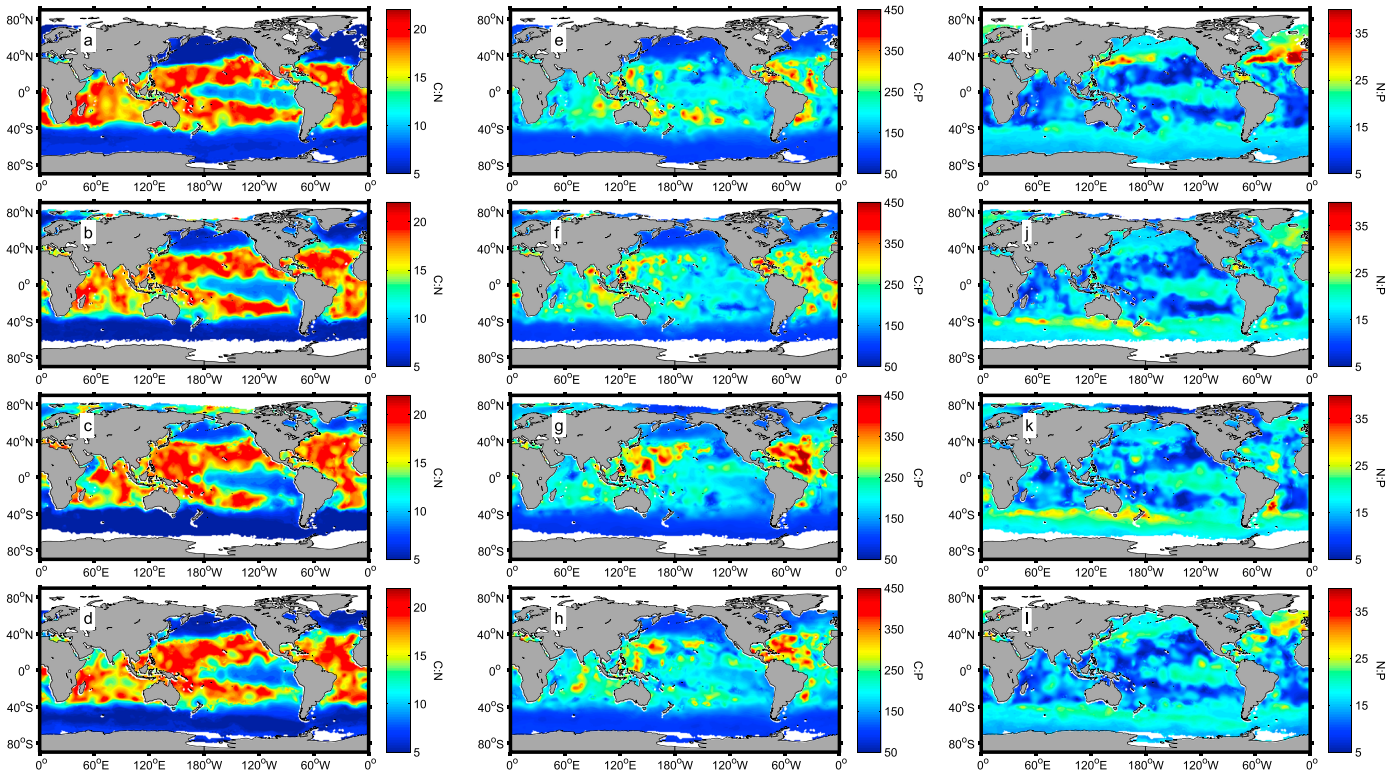

Figure 2. Global patterns of the model-derived phytoplankton cellular (a–d) C:N, (e–h) C:P, and (i–l) N:P ratio (mol mol^{-1}) in the ocean. Each image is a 3 month average composite: (Figures 2a, 2e, and 2i) January–March, (Figures 2b, 2f, and 2j) April–June, (Figures 2c, 2g, and 2k) July-September, and (Figures 2d, 2h, and 2l) October-December.

and subtropical ocean shows C:P ratios of about 200 mol mol^{-1}. Higher latitudes show the lowest C:P of ~100 mol mol^{-1} (Figures 2e–2h), which is close to the Redfield ratio of 106 mol mol^{-1}.

Figure 3a compares our modeled C:P latitudinal pattern to observations. Black asterisks in Figure 3a show the lognormal average of the observations of particulate organic carbon:particulate organic phosphorus (POC:POP) ratios for each latitudinal band from *Martiny et al.* [2013b]. To make our results more comparable with observations, modeled C:P in Figure 3a are also calculated as lognormal longitudinal averages. There is a close agreement between model and observations, showing low C:P at high latitudes, and vice versa, with the lowest C:P located in southern high latitudes. The agreement in the C:P trend is an encouraging result, as *Martiny et al.* [2013b] indicate that the contribution of living phytoplankton and bacteria to the POP pool in their data set was around 98%, suggesting that the C:P diagnosed from the bulk particulate organic matter (POM) data could be viewed as representative of phytoplankton C:P.

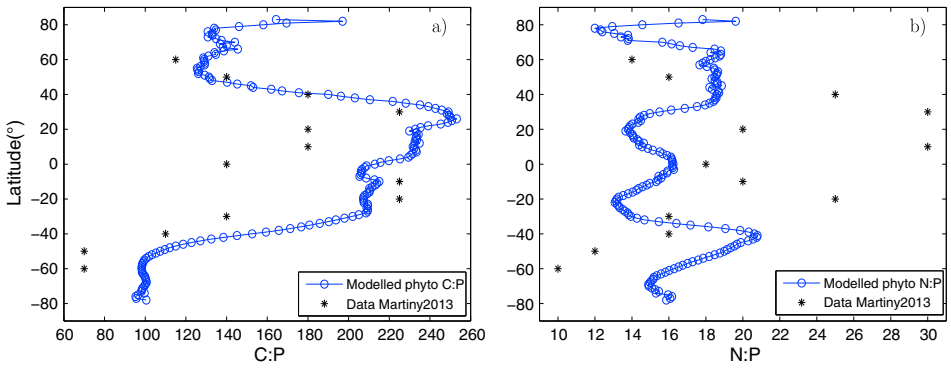

Figure 3. Annual lognormal (a) C:P and (b) N:P latitudinal patterns. Black asterisks show lognormal averages of POC:POP and PON:POP observations for each latitudinal band, presented in Figure 2 of *Martiny et al.* [2013b].

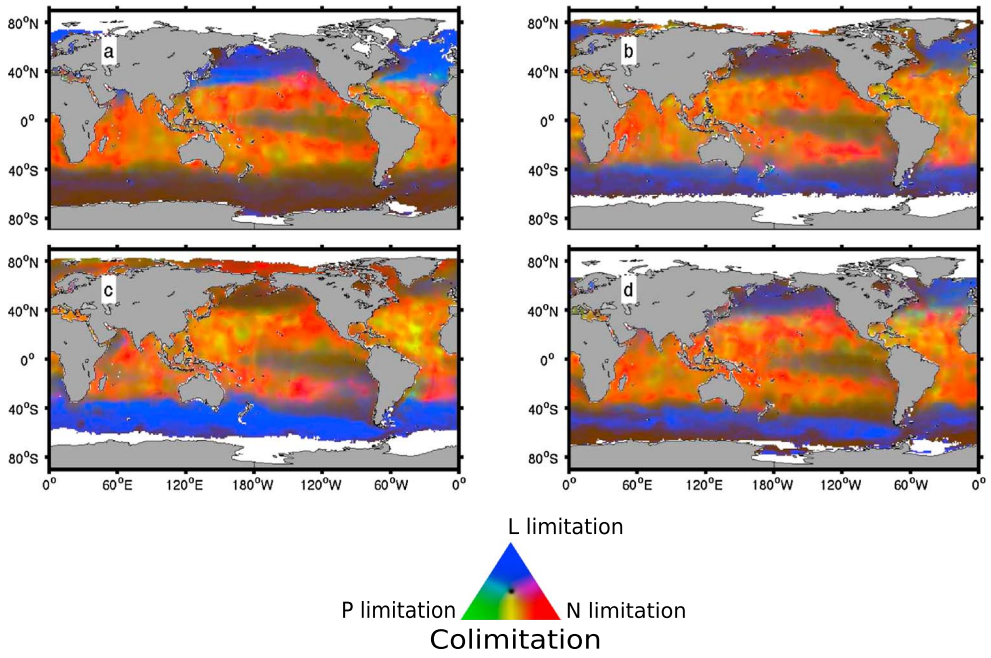

Figure 4. Diagnosed seasonal oceanic N, P, and light colimitation of marine phytoplankton. The maps are red-green-blue (RGB) composites of N limitation (red), P limitation (green), and light (L) limitation (blue). Colimitation is reflected by the combination of colors: purple (N-light colimitation), yellow (N-P colimitation), and cyan (P-light colimitation). Bright colors indicate limitation, whereas dark colors indicate saturation (no limitation). Seasonal images are 3 month average composites: (a) January–March, (b) April–June, (c) July–September, and (d) October–December.

Our simulated N:P ratio (Figures 2i–2l) shows relatively weak seasonal and spatial trends. In general, the lowest N:P are found in oligotrophic areas due to the effect of N limitation, while highest N:P is found in the eastern north Atlantic and western north Pacific, during January–March (Figure 2i). The latitudinal distribution of our modeled N:P (lognormal averages) across all seasons is shown in Figure 3b, together with bulk POM data from *Martiny et al.* [2013b]. Modeled N:P ratios show a rather unclear latitudinal trend when compared with observations, varying between 12 and 22. The lowest longitudinally averaged N:P values are obtained at high latitudes around 80°N (N:P∼12), followed by an increase between 60°N and 30°N, and a decrease between 30°N and 30°S, where the phytoplankton N:P stays close to 16 (the Redfield N:P ratio). Between 40°S and 80°S our predicted N:P increases to 22 and decreases again to 16. The POM-derived observations present a much wider range of variation in the N:P ratios, between 10 and 30, with lowest values at high latitudes and vice versa. Our modeled phytoplankton N:P presents some features that are similar to those of *Martiny et al.* [2013b], such as low values in higher northern latitudes, and a slight increase toward lower latitudes. However, the main discrepancy between model and observations is the high N:P values obtained at subtropical regions in PON:POP data, which results in a much clearer low-to-high N:P latitudinal pattern. A possible explanation for this mismatch could be that data on particulate organic matter (POM) might not accurately represent the stoichiometry of phytoplankton, which is what our model analysis describes. In fact, *Martiny et al.* [2013a] analyzed phytoplankton and bulk particulate C:N ratios and found that the phytoplankton C:N was almost twice the bulk value in the western North Atlantic. This implies a relatively low N content of the phytoplankton compared to bulk POM, so that at least part of the N:P discrepancy between our model and the observations of *Martiny et al.* [2013b] might reflect true differences between phytoplankton and bulk POM composition.

Further model development and inclusion of other processes and relevant limiting nutrients in the model physiological dynamics could further reconcile the model and in situ observations. For example, we expect the inclusion of diazotrophy to increase the predicted N:P ratio [*Krauk et al.*, 2006] in midlatitude regions, where nitrogen fixation may be important [*Gruber and Sarmiento*, 1997]. Accounting for other nitrogen sources not represented in the climatology, such as ammonium, could also affect nitrogen uptake [*Dortch*, 1982] in low latitudes and hence phytoplankton N:P ratios. Iron can also limit nitrogen assimilation and

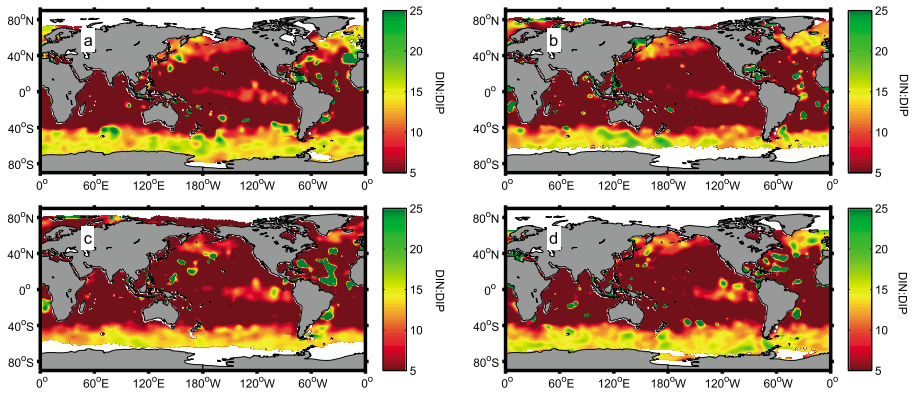

Figure 5. Seasonal oceanic DIN:DIP ratio calculated from WOA09. Each image is a 3 month average composite: (a) January–March, (b) April–June, (c) July–September, and (d) October–December.

carbon fixation, which can potentially alter our predicted cell quotas in high-nutrient, low-chlorophyll (HNLC) regions (see below).

3.2. Light and Nutrient Colimitation

Using L_I together with the N and P limitation indices L_N and L_P diagnosed from the model, we produced seasonal light and nutrient colimitation maps on a 1° × 1° grid for the global ocean (Figure 4). These composite maps of N (red), P (green), and light (blue) (co)limitation identify the roles of each of these factors in controlling phytoplankton growth according to our model. Red and blue areas indicate N and light limitation, respectively, while green areas indicate P limitation. The combination of red and blue (purple areas) indicates nitrogen-light colimitation; red and green (yellow areas) indicates nitrogen-phosphorus colimitation, while green and blue (cyan areas) indicates phosphorus-light colimitation. Brighter colors indicate strong (co)limitation, while dark colors suggest absence of limitation (by either N, P, or light).

The colimitation maps (Figure 4) indicate a dominance of N limitation and N-P colimitation (red and yellow areas respectively) over large parts of the tropical oceans between 40°N and 40°S. Strong N limitation appears over the north and south eastern subtropical Pacific. The Atlantic Ocean, particularly above the equator, shows strong N-P colimitation, which is most severe during the period of July–September (Figure 4c). The eastern equatorial Pacific displays a general lack of limitation, resulting from increased DIN and DIP concentrations due to the equatorial upwelling, which injects nutrients into the surface ocean. The strongest seasonality in limitation patterns is observed at high latitudes, especially over the Pacific Ocean. Here light limitation is present in winter in January–March, followed by generally low light, N, and P limitation in April–June. Nutrient (N-P) colimitation appears in July–September, particularly north of 40°N, while slight light limitation occurs again during October–December.

Contrary to northern latitudes, there is no sign of clear N or P limitation for the Southern Ocean in our colimitation maps. No limitation is observed during the austral summer (January–March), while clear light limitation is present during winter (July–September). Over the periods April–June and October–December, the Southern Ocean appears in general not limited, except for some areas showing exclusive light limitation (Figure 4).

Low C:N and C:P ratios diagnosed for the Southern Ocean (Figure 2) suggest absence of N or P limitation, which is consistent with our expectation for the real ocean for which iron is well established as the primary limiting nutrient in this region [*Martin et al.*, 1990; *Boyd et al.*, 2007]. Light limitation is only clearly evident during austral winter, as expected due to low irradiance and deep mixed layers. Iron regulates the assimilation of nitrate and is an important constituent of the photosynthetic electron transport chain [*Geider and LaRoche*, 1994]. As iron limitation interferes with the ability of phytoplankton cells to photoacclimate [*Greene et al.*, 1992], and our model does not explicitly account for the effects of iron, the results presented here should actually underestimate true light limitation under iron-limited conditions. Hence, following the idea of a chain of (co)limitations, light could be a strongly limiting factor of phytoplankton growth in this region [*Mitchell et al.*, 1991; *Nelson and Smith*, 1991] even if iron dynamics are considered.

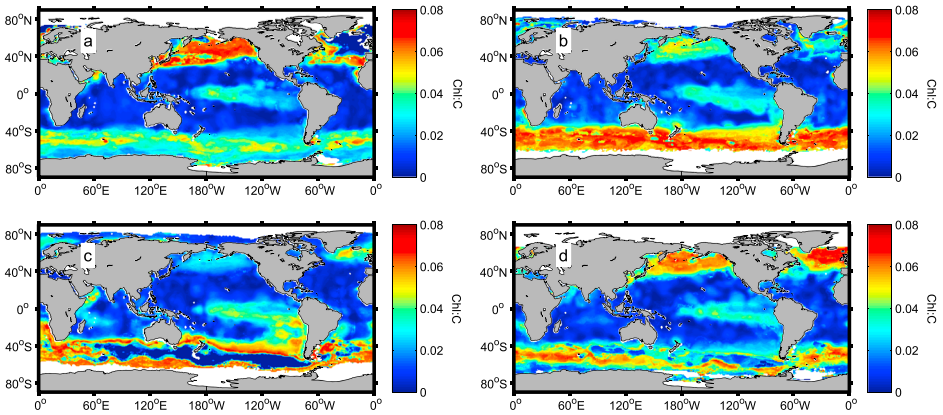

Figure 6. Global patterns of the model-based phytoplankton Chl:C ratio in the ocean. Each image is a 3 month average composite: (a) January–March, (b) April–June, (c) July–September, and (d) October–December.

Another important factor to take into account is the effect of iron on the nitrogen cell quota and thus phytoplankton cellular stoichiometry. As discussed above, the neglect of iron in the current version of the chain model [*Pahlow et al.*, 2013], likely results in an overestimation of the N:P ratio in areas where iron is an important limiting agent of phytoplankton growth, such as the Southern Ocean. Nitrate utilization can be limited by low ambient iron concentrations, as iron compounds serve as co-factors in the reduction from nitrate via nitrite to ammonium [*Timmermans et al.*, 1994]. Hence, we expect that the inclusion of iron in the model cellular dynamics should result in a reduction of the N:P ratio, particularly south of 40°S, where also the lowest N:P ratios are found in the POM data.

The results of our model-derived colimitation analysis can be compared against a traditional analysis of inorganic nutrient ratios in the surface layer. Shown in Figure 5 are seasonal global maps of DIN:DIP ratios extracted from WOA09. The DIN:DIP maps are similar to our colimitation maps in that both show a dominance of N as the main limiting nutrient, particularly in low latitudes. However, while indicating the relative proportion of dissolved N and P in the water, the DIN:DIP ratio does not allow assessing the absolute intensity of the individual nutrient limitation or colimitation. Conversely, our analysis is able to show that P does have a significant importance as a colimiting nutrient for nondiazotrophic phytoplankton, particularly in the Atlantic Ocean. Changes in seasonal colimitation at high latitudes are not evident in the DIN:DIP maps, while our colimitation analysis shows a clear transition from light to N-P colimitation from winter to summer. For the Southern Ocean, both maps suggest neither N nor P limitation (DIN:DIP $\sim$ 16), but our model-based analysis is able to detect strong light limitation during winter. If iron was considered, it would likely turn out as another strong limiting factor in the Southern Ocean. As iron limitation interferes with photoacclimation, we expect that light limitation could be stronger than that shown in Figure 4. Iron limitation also prevents nitrate assimilation, which in turn, should increase C:N ratios and thereby cause N limitation in this region. Consequently, we expect the net effect of iron limitation in terms of our analysis to be enhanced N light colimitation.

Our global patterns generally agree with previous model studies of nutrient limitation in the ocean. *Aumont et al.* [2003] showed that N or P limitation is mainly restricted between 40°N and 40°S for nanophytoplankton and diatoms. However, *Aumont et al.* [2003] cannot differentiate between N and P limitation, thus, a direct comparison with our results is not possible. *Moore et al.* [2002] employed a similar approach based on cellular quotas, but noted that nutrient limitation was difficult to assess during times of strong light limitation due to its effect on cell quotas. This shortcoming is overcome in our analysis by diagnosing the effect of light limitation independently (1-S_I, where S_I quantifies the degree of light saturation of the cellular light-harvesting apparatus), and comparing it with N and P limitation. Nevertheless, *Moore et al.* [2002] also find strong N limitation in midocean gyres and substantial P limitation in the north Atlantic and western north Pacific. An important difference between previous model-based nutrient limitation analyses and our model is that most previous models are based on static formulations of the Michaelis-Menten equation applied to different nutrients in order to identify the limiting nutrient. In the chain model used here, colimitation exists in the sense that P availability in the cell directly affects the cell's ability to assimilate N, which in turn limits carbon fixation. Furthermore, and perhaps more relevant in terms of future ocean

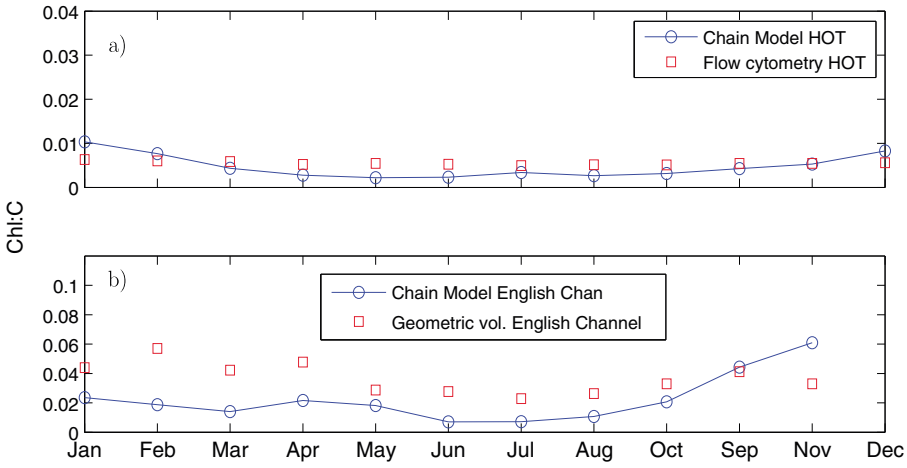

Figure 7. Monthly patterns of phytoplankton Chl:C ratio in the (a) Hawaii Ocean Time series (HOT), and (b) English Channel. Red squares are flow cytometry data for HOT [*Winn et al.*, 1995] scaled to Chl:C [*Westberry et al.*, 2008] and Chl:C estimations from phytoplankton cell volume through cell geometry analysis for the English channel [*Llewellyn et al.*, 2005]. Blue circles connected with lines are model results. Model outputs are obtained using the Default parameter set.

escenarios, our optimality-based approach allows for variable nutrient affinity, which depends on both the intracellular and external nutrient concentration. This permits the representation of more flexible nutrient acquisition dynamics and allows for acclimation of phytoplankton to different environmental conditions.

3.3. Chlorophyll to Carbon Ratio

Our model-based colimitation maps predict N limitation and N-P colimitation in midlatitudes and a seasonal succession of light limitation and N-P colimitation in northern latitudes. The eastern equatorial Pacific and the Southern Ocean show a general absence of limitation, except for the austral winter, where the Southern Ocean appears clearly light limited. Considering N and P limitation, our results are in agreement with recently reviewed experimental evidence [*Moore et al.*, 2013]. These spatial and temporal environmental patterns are also reflected in the modeled chlorophyll to carbon ratio (Chl:C) ratio, which serves as a physiological indicator of phytoplankton (Figure 6). The Chl:C ratio integrates the combined effects of N, P, and light limitation, driven by the requirements of N for CO_2 fixation and Chl for light harvesting. Low light conditions together with high-nutrient concentrations produce the highest Chl:C ratios, as cells photo-acclimate by increasing the Chl cell quota. This is only possible when sufficient nitrogen is available to meet the demand of the enzymatic machinery that processes the energy acquired through light harvesting [*Falkowski and Raven*, 1997]. Nitrogen is also required in pigment-bound proteins and used for pigment synthesis, which is accounted for in the model as part of the N allocated to the generic light-harvesting compartment. Lowest Chl:C ratios occur when light levels are high, as cells down-regulate the synthesis of Chl, or when low nitrogen concentrations limit Chl synthesis and hence photo-acclimation. Extreme low light conditions, however, will increase the cost of Chl synthesis significantly, resulting in Chl:C ratios = 0 (equation 5). This occurs in our model-based results during winter (July–September) in some areas of the Southern Ocean (Figure 6c), where despite high nutrient availability, light is too low for phytoplankton growth. The range of predicted Chl:C ratios is then the result of a balance between the need and the possibility for photoacclimation as driven by the availability of nutrients and light.

As the chlorophyll to carbon ratio reflects phytoplankton cellular physiology under nutrient and/or light limitation [*Geider et al.*, 1998], we evaluate our model-based results against available observations of seasonal Chl:C variations. We chose Chl:C ratios to validate our results because it appears to be more directly linked to phytoplankton growth than other cellular ratios (e.g., N:P) [*Terry et al.*, 1983, 1985]. Also, observations on Chl:C found in the literature are more directly related to phytoplankton cellular components and not total POM, as is often the case for N:P measurements. Data were obtained from fluorescence measurements at the Hawaii Ocean Time series (HOT) [*Winn et al.*, 1995], scaled to Chl:C [*Westberry et al.*, 2008] and cell volumes estimated from cell geometry in the English Channel [*Llewellyn et al.*, 2005]. At both sites, the temporal evolution of the observed Chl:C ratios can be reproduced reasonably well, although the model slightly underestimates the Chl:C at the English Channel location, particularly during the first months of the

Table 2. Model Symbols in Appendix A

Symbol	Description
f_N	Fraction of f_V Q^N allocated for N
f_V	Fraction of Q^N allocated for nutrient acquisition
I_g	Median mixed layer light level (E m^{-2} d^{-1})
μ	Net growth rate (d^{-1})
PAR	Photosynthetically active radiation (E m^{-2} d^{-1})
Q^N	N:C ratio (mol N mol C^{-1})
Q_s^N	Partial N quota bound in structural protein (mol N mol C^{-1})
R	Respiration (d^{-1})
R^{Chl}	Cost of photosynthesis (d^{-1})
S_I	Light saturation
TEMP	Temperature (°C)
V^C	C fixation rate (mol C mol C^{-1} d^{-1})
V^N	N assimilation rate (mol N mol C^{-1} d^{-1})
V^P	P assimilation rate (mol P mol C^{-1} d^{-1})
V_0^C	Potential C fixation rate (mol C mol C^{-1} d^{-1})
V^N	Local potential N assimilation rate (mol N mol C^{-1} d^{-1})
V^P	Local potential P assimilation rate (mol P mol C^{-1} d^{-1})
ζ^N	Cost of DIN uptake (mol C mol N^{-1})

year (Figure 7). The parameter set used for this validation exercise is the same as for all the modeled cell quotas and limitation indices outputs presented above (parameter set "Default," Table 1).

3.4. Model Sensitivity

All model results presented here have been obtained from the chain model using the Default parameters in Table 1. In order to examine the sensitivity of our model predictions to different parameter settings, model outputs were also obtained for two additional parameter sets, Case I and Case II, which were selected to cover much of the range of parameters in Table 2 of *Pahlow et al.* [2013]. For these sensitivity experiments a regional breakdown of the results similar to that of *Behrenfeld et al.* [2005] was used. Monthly model outputs were produced for different regions of the global ocean, characterized by five variance levels based on standard deviations of seasonal Chl, calculated from Chl satellite data (mg m^{-3}) obtained from MODIS (http://oceancolor.gsfc.nasa.gov/), from January 2005 to December 2010 (Figure 8). The variance levels are defined as: L0 = 0 < SD_{Chl} <0.004 mg Chl m^{-3}, L1 = 0.004 <SD_{Chl} <0.007 mg Chl m^{-3}, L2 = 0.007< SD_{Chl} <0.03 mg Chl m^{-3}, L3 = 0.03<SD_{Chl} <0.3 mg Chl m^{-3}, L4 = SD_{Chl} >0.3 mg Chl m^{-3}. The precise cutoff values of these regions are not critical and were simply chosen to yield regions consistent with large-scale ocean circulation and pigment features [*Behrenfeld et al.*, 2005].

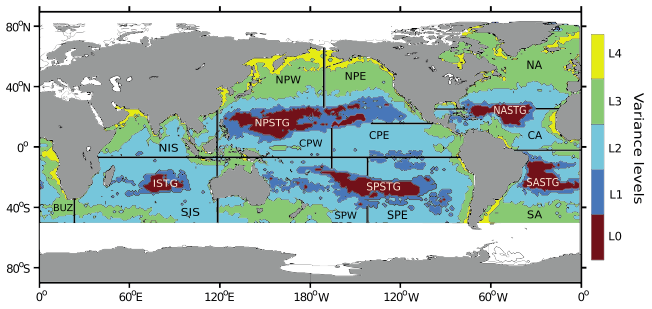

Figure 8. Map of 17 areas of the global ocean divided according to their geographical position. The resulting areas were subdivided based on their seasonal variability of surface Chl (levels L0 to L4), estimated from the satellite sensor MODIS (http://oceancolor.gsfc.nasa.gov/) between 2005 and 2010. The subdivision of the 17 geographical areas produced 12 areas of high Chl variability that only have Chl variance levels L2, L3, and L4: North Pacific West (NPW), North Pacific East (NPE), Central Pacific West (CPW), Central Pacific East (CPE), South Pacific West (SPW), South Pacific East (SPE), North Atlantic (NA), Central Atlantic (CA), South Atlantic (SA), Benguela Upwelling Zone (BUZ), North Indian Sea (NIS), and South Indian Sea (SIS); and five areas of low Chl variability that only have levels L0 and L1: North Pacific Sub-Tropical Gyre (NPSTG), South Pacific Sub-Tropical Gyre (SPSTG), North Atlantic Sub-Tropical Gyre (NASTG), South Atlantic Sub-Tropical Gyre (SASTG), and Indian Subtropical Gyre (ISTG).

Figure 9 contrasts differences between the three parameter sets Default (blue), Case I (red), and Case II (green) with differences between geographical areas for Chl:C, L_N, L_P, and L_I. Figures 9a–9d show two selected areas of the Atlantic Ocean (L3-North Atlantic and L0-North Atlantic Sub-Tropical Gyre), while Figures 9e–9h present two selected areas of the Pacific Ocean (L3-North Pacific East and L2-Central Pacific East). Differences between model results obtained with the distinct

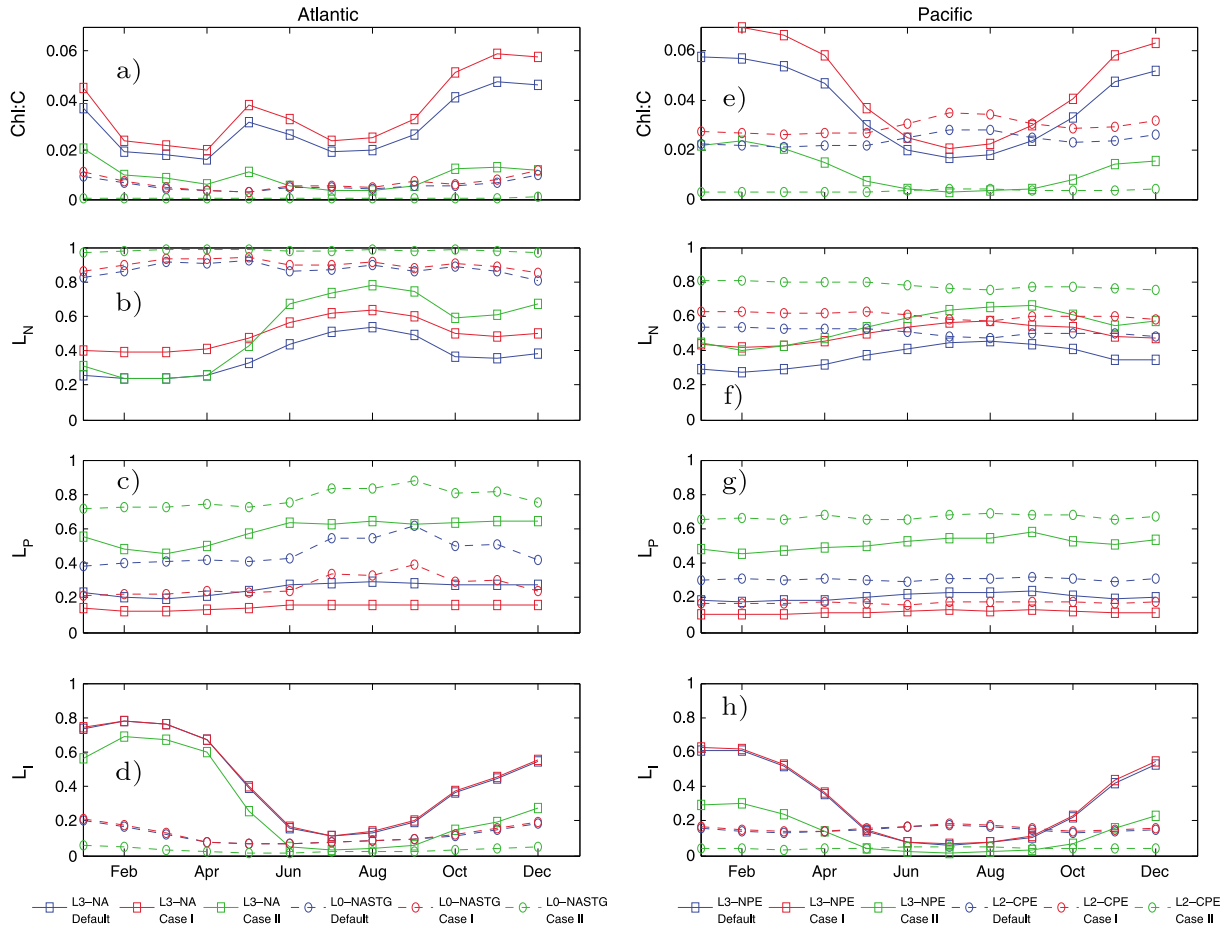

Figure 9. Model sensitivity experiments for parameter settings "Default" (blue), "Case I" (red), and "Case II" (green). Plotted oceanic areas in the Atlantic ocean (a–d): L3-North Atlantic (squares and continuous line) and L0-North Atlantic Sub-Tropical Gyre (circles and dashed line). Plotted oceanic areas in the Pacific ocean (e–h): L3-North Pacific East (squares and continuous line) and L2-Central Pacific East (circles and dashed line). Chl:C (Figures 9a and 9e) is the chlorophyll to carbon ratio of phytoplankton. (Figures 9b and 9f) L_N, (Figures 9c and 9g) L_P, and (Figures 9d and 9h) L_I are the nitrogen, phosphorus, and light limitation indices, respectively.

parameter sets are generally smaller than differences between geographical regions in each model simulation. For the Chl:C ratio, lower values are obtained for the Case II simulation due to a higher carbon cost for photosynthesis (ζ^{Chl}) and a significantly higher light absorption coefficient (α). L_N shows relatively small differences between runs. Case II presents overall the highest N limitation due to a significantly lower nutrient affinity (A_0) with respect to Case I and Default. For L_P, Case II appears again as the most limited simulation, as a result of the combination of a low A_0 and the highest phosphorus subsistence quota (Q_0^P) of all three simulations. Stronger light limitation is found in the Default and Case I simulations due to lower light absorption coefficients (α), which reduce the phytoplankton efficiency of C assimilation. In general, changes in the parameters mostly affect the magnitude of the limitation indices and Chl:C ratio, but not the seasonal trend of the results. The model's seasonal behavior is in all cases determined by the variability of the forcing (nutrient and light) data. Overall spatial patterns of nutrient and light colimitation remain unaltered regardless of which set of parameters is used.

4. Conclusions

Our combined model-data analysis suggests strong N limitation and N-P colimitation in the tropical and subtropical ocean, and seasonal light limitation and N-P colimitation in Northern Hemisphere high latitudes. The eastern equatorial Pacific shows an overall lack of limitation by either N, P, or light, while the Southern Ocean appears strongly light limited during winter. Our colimitation analysis is able to describe the combined effects of N, P, and light (co)limitation, which cannot be achieved with a traditional inspection of

DIN:DIP ratios. However, our model-based results yield to some extent similar patterns as limitation estimates inferred from oceanic DIN:DIP ratios with respect to the Redfield ratio. This comes as a surprising result, given that our mechanistic model allows for flexible rather than Redfield phytoplankton stoichiometry. There is no clear reason why optimality-derived cell quotas should approach the Redfield N:P ratio (~16). However, while our predicted N:P varies widely globally (around 5 to 40 mol mol^{-1}), a pointwise average among all seasons of our predicted phytoplankton N:P ratios yields a global N:P of 16. This could suggest that although optimality-derived individual phytoplankton cell quotas do not approach any particular common stoichiometry, the present distribution of available dissolved N and P in the surface ocean induces the optimality-derived N:P ratio of global phytoplankton to have a mean value close to Redfield stoichiometry.

A shortcoming of our current model is the neglect of iron limitation. Including iron dynamics in our analysis could have an important effect on N:P ratios in HNLC regions such as the Southern Ocean. Currently we are not aware of experimental data suitable for including iron (co)limitation in our optimality-based model concept. Apart from these HNLC regions, we believe that the neglect of iron limitation should not induce major changes in the relative distribution of N, P, and light colimitation areas, as these are estimated from cell quotas relative to phytoplankton biomass (and not from N:P ratios). The relative importance of N, P, and light in limiting phytoplankton growth diagnosed here by combining observations and an optimal-growth model, thus provides a useful constraint on models used to predict future marine biological production under changing environmental conditions.

Appendix A: Supplementary Material

S.1 Overview of the Chain Model

In the optimality-based phytoplankton growth model of *Pahlow et al.* [2013], growth (μ) is described as the difference between C fixation (V^c) and respiration (R),

$$\mu = V^c - R \tag{S.1}$$

V^c is a function of N cell quota (Q^N), the potential CO_2 fixation rate (V_0^c), and PAR. PAR in this work is used to quantify I_g (equation (1)). The effect of light limitation is then estimated by the degree of light saturation of the cellular light-harvesting apparatus, S_I (equation (2)). The C-fixation rate is then defined as,

$$V^c = V_0^c \left(1 - \frac{Q_s^N}{Q^N} - f_V\right) S_I \tag{S.2}$$

where f_V is the fraction of cellular N allocated for nutrient acquisition, and Q_s^N represents cellular N bound in structural protein. Respiration comprises the cost of photosynthesis (R^{ChI}) and the cost of N assimilation ($\zeta^N V^N$) assumed to be proportional to N assimilation (V^N),

$$R = \zeta^N V^N + R^{ChI} \tag{S.3}$$

N allocated for nutrient acquisition ($f_v Q^N$) is further divided between DIN and DIP acquisition via another allocation factor (f_N):

$$V^N = f_V f_N V_*^N \qquad V^P = f_V (1 - f_N) V_*^P \tag{S.4}$$

where V_*^N and V_*^P are potential rates of N and P uptake as functions of potential uptake rates, V_0^N, V_0^P, and affinity, A_0.

The allocation factors f_V and f_N are calculated to maximize net balanced growth rate.

S.2 Temperature Dependence

Since the original model [*Pahlow et al.*, 2013] does not include temperature, we introduced a temperature dependence [*Eppley*, 1972] of the maximum rate parameters as follows:

$$V_0^C, V_0^N, V_0^P = 1.4 * 1.066^{TEMP}$$

Acknowledgments

We wish to thank M. Behrenfeld and R. O'Malley for sharing their expertise and providing helpful insights on satellite inputs and the computation of the median mixed layer light level (I_g). The research leading to these results has received funding from the European Community's Seventh Framework Programme FP7/2007-2013, Space Theme, under grant agreement 282723 (OSS2015). This work is also a contribution of the Sonderforschungsbereich 754 "Biogeochemistry Interactions in the Tropical Ocean" (www.sfb754.de).

References

Ågren, G. I (2004), The C:N:P stoichiometry of autotrophs—Theory and observations, *Ecol. Lett.*, *7*, 185–191, doi:10.1111/j.1461-0248.2004.00567.x.

Aumont, O., E. Maier-Reimer, S. Blain, and P. Monfray (2003), An ecosystem model of the global ocean including Fe, Si, P colimitations, *Global Biogeochem. Cycles*, *17*(2), 1060, doi:10.1029/2001GB001745.

Behrenfeld, M. J., E. Boss, D. A. Siegel, and D. M. Shea (2005), Carbon-based ocean productivity and phytoplankton physiology from space, *Global Biogeochem. Cycles*, *19*, GB1006, doi:10.1029/2004GB002299.

Boyd, P. W., et al. (2007), Mesoscale iron enrichment experiments 1993–2005: Synthesis and future directions, *Science*, *315*, 612–617, doi:10.1126/science.1131669.

Cullen, J., and M. Lewis (1988), The kinetics of algal photoadaptation in the context of vertical mixing, *J. Plankton Res.*, *10*(5), 1039–1063.

Dortch, Q. (1982), The interaction between ammonium and nitrate uptake in phytoplankton, *Mar. Ecol. Prog. Ser.*, *61*, 183–201.

Droop, M. R. (1983), 25 Years of algal growth kinetics: A personal view, *Bot. Mar.*, *26*, 99–112.

Eppley, R. W. (1972), Temperature and phytoplankton growth in the sea, *Fish. Bull.*, *70*(4), 1063–1085.

Falkowski, P. G., and J. Raven (1997), *Aquatic Photosynthesis*, Blackwell Science Ltd., Oxford, U. K.

Fanning, K. A. (1992), Nutrient provinces in the sea: Concentration ratios, reaction rate ratios, and ideal covariation, *J. Geophys. Res.*, *97*(C4), 5693–5712.

Flynn, K. J. (2010), Do external resource ratios matter?, *J. Mar. Syst.*, *83*, 170–180, doi:10.1016/j.jmarsys.2010.04.007.

Geider, R. J., and J. LaRoche (1994), The role of iron in phytoplankton photosynthesis, and the potential for iron-limitation of primary productivity in the sea, *Photosynth. Res.*, *39*, 275–301.

Geider, R. J., and J. LaRoche (2002), Redfield revisited: Variability of C:N:P in marine microalgae and its biochemical basis, *Eur. J. Phycol.*, *37*, 1–17.

Geider, R. J., H. L. MacIntyre, and T. Kana (1998), A dynamic regulatory model of phytoplanktonic acclimation to light, nutrients, and temperature, *Limnol. Oceanogr.*, *43*, 679–694.

Goldman, J., J. McCarthy, and D. Peavey (1979), Growth rate influence on the chemical composition of phytoplankton in oceanic waters, *Nature*, *279*, 210–215.

Greene, R. M., R. J. Geider, Z. Kolber, and P. G. Falkowski (1992), Iron-induced changes in light harvesting and photochemical energy conversion processes in eukaryotic marine algae, *Plant Physiol.*, *100*, 565–75.

Gruber, N., and J. L. Sarmiento (1997), Global patterns of marine nitrogen fixation and denitrification, *Global Biogeochem. Cycles*, *11*(2), 235–266.

Healey, F. P. (1985), Interacting effects of light and nutrient limitation on the growth rate of *Synechococcus linearis* (cyanophyceae), *J. Phycol.*, *21*, 134–146.

Klausmeier, C., E. Litchman, T. Daufresne, and S. Levin (2004), Optimal nitrogen-to-phosphorus stoichiometry of phytoplankton, *Nature*, *429*, 171–174, doi:1.1029/2001GL014649.

Körtzinger, A., W. Koeve, P. Kähler, and L. Mintrop (2001), C:N ratios in the mixed layer during the productive season in the northeast Atlantic Ocean, *Deep Sea Res. Part I*, *48*, 661–688.

Krauk, J. M., T. A. Villareal, J. A. Sohm, J. P. Montoya, and D. G. Capone (2006), Plasticity of N:P ratios in laboratory and field populations of *Trichodesmium* spp, *Aquat. Microb. Ecol.*, *42*, 243–253.

Laws, E. A., and T. T. Bannister (1980), Nutrient and light limited growth of *Thalassiosira fluviatilis* in continuous culture, with implications for phytoplankton growth in the ocean, *Limnol. Oceanogr.*, *25*, 457–473.

Levitus, S. (1982), Climatological atlas of the world ocean, *NOAA Professional Paper 13*, U.S. Government Printing Office, Washington, D. C.

Llewellyn, C. A., J. R. Fishwick, and J. C. Blackford (2005), Phytoplankton community assemblage in the English Channel: A comparison using chlorophyll a derived from HPLC-CHEMTAX and carbon derived from microscopy cell counts, *J. Plankton Res.*, *27*(1), 103–119, doi:10.1093/plankt/fbh158.

Martin, J., R. M. Gordon, and S. E. Fitzwater (1990), Iron in Antarctic waters, *Nature*, *345*, 156–158, doi:10.1038/345156a0.

Martiny, A. C., J. A. Vrugt, F. W. Primeau, and M. W. Lomas (2013a), Regional variation in the particulate organic carbon to nitrogen ratio in the surface ocean, *Global Biogeochem. Cycles*, *27*(3), 723–731, doi:10.1002/gbc.20061.

Martiny, A. C., C. T. A. Pham, F. W. Primeau, J. A. Vrugt, J. K. Moore, S. A. Levin, and M. W. Lomas (2013b), Strong latitudinal patterns in the elemental ratios of marine plankton and organic matter, *Nat. Geosci.*, *6*, 279–283, doi:10.1038/ngeo1757.

Mitchell, B. G., E. A. Brody, O. Holm-Hansen, C. McClain, and J. Bishop (1991), Light limitation of phytoplankton biomass and macronutrient utilization in the Southern Ocean, *Limnol. Oceanogr.*, *36*(8), 1662–1677.

Moore, C. M., et al. (2013), Processes and patterns of oceanic nutrient limitation, *Nat. Geosci.*, *6*, 701–710, doi:10.1038/ngeo1765.

Moore, J. K., S. C. Doney, D. M. Glover, and I. Y. Fung (2002), Iron cycling and nutrient-limitation patterns in surface waters of the World Ocean, *Deep Sea Res. Part II*, *49*, 463–507.

Nelson, D. M., and W. Smith (1991), Sverdrup revisited: Critical depths, maximum chlorophyll levels, and the control of Southern Ocean productivity by the irradiance-mixing regime, *Limnol. Oceanogr.*, *36*(8), 1650–1661.

Pahlow, M. (2005), Linking chlorophyll-nutrient dynamics to the Redfield N:C ratio with a model of optimal phytoplankton growth, *Mar. Ecol. Prog. Ser.*, *287*, 33–43.

Pahlow, M., and A. Oschlies (2013), Optimal allocation backs Droop's cell-quota model, *Mar. Ecol. Prog. Ser.*, *473*, 1–5, doi:10.3354/meps10181.

Pahlow, M., H. Dietze, and A. Oschlies (2013), Optimality-based model of phytoplankton growth and diazotrophy, *Mar. Ecol. Prog. Ser.*, *489*, 1–16, doi:10.3354/meps10449.

Quigg, A., Z. V. Finkel, A. J. Irwin, Y. Rosenthal, T.-Y. Ho, J. R. Reinfelder, O. Schofield, F. M. M. Morel, and P. G. Falkowski (2003), The evolutionary inheritance of elemental stoichiometry in marine phytoplankton, *Nature*, *425*, 291–294, doi:10.1038/nature01953.

Redfield, A. (1934), On the proportions of organic derivatives in sea water and their relation to the composition of plankton, in *James Johnstone Memorial Volume*, edited by R. Daniel, pp. 176–192, Univ. Press of Liverpool, Cambridge, U. K.

Rhee, G. (1978), Effects of N:P atomic ratios and nitrate limitation on algal growth, cell composition, and nitrate uptake, *Limnol. Oceanogr.*, *23*(1), 10–25.

Smith, S. L., M. Pahlow, A. Merico, and K. W. Wirtz (2011), Optimality-based modeling of planktonic organisms, *Limnol. Oceanogr.*, *56*(6), 2080–2094, doi:10.4319/lo.2011.56.6.2080.

Sterner, R. W., and J. J. Elser (2002), Ecological stoichiometry: The biology of elements from molecules to the biosphere, Princeton Univ. Press, Princeton, N. J.

Terry, K., J. Hirata, and E. Laws (1983), Light limited growth of two marine strains of the marine diatom *Phaeodactylum tricornutum* Bohlin: Chemical composition, carbon partitioning, and the diel periodicity of physiological processes, *J. Exp. Mar. Biol. Ecol.*, *68*, 209–227.

Terry, K., J. Hirata, and E. Laws (1985), Light-, nitrogen-, and phosphorus-limited growth of *Phaeodactylum tricornutum* Bohlin strain tfx-1: Chemical composition, carbon partitioning, and the diel periodicity of physiological processes, *J. Exp. Mar. Biol. Ecol.*, *86*, 85–100.

Timmermans, K., W. Stolte, and H. Baar (1994), Iron-mediated effects on nitrate reductase in marine phytoplankton, *Mar. Biol.*, *121*, 389–396.

Weber, T., and C. Deutsch (2012), Oceanic nitrogen reservoir regulated by plankton diversity and ocean circulation, *Nature*, *489*, 419–22, doi:10.1038/nature11357.

Westberry, T., M. J. Behrenfeld, D. A. Siegel, and E. Boss (2008), Carbon-based primary productivity modeling with vertically resolved photoacclimation, *Global Biogeochem. Cycles*, *22*, GB2024, doi:10.1029/2007GB003078.

Winn, C. D., L. Campbell, J. R. Christian, R. M. Letelier, D. V. Hebel, J. E. Dore, L. Fujieki, and D. M. Karl (1995), Seasonal variability in the phytoplankton community of the North Pacific Subtropical Gyre, *Global Biogeochem. Cycles*, *9*, 605–620, doi:10.1029/95GB02149.

Wu, J., W. Sunda, E. A. Boyle, and D. M. Karl (2000), Phosphate depletion in the North Atlantic Ocean, *Science*, *289*, 759–762, doi:10.1126/science.289.5480.759.